JGR Oceans

RESEARCH ARTICLE
10.1029/2019JC015863

Tidal Effect on Water Export Rate in the Eastern Shelf Seas of China

Lei Lin[1], Dongyan Liu[1], Xinyu Guo[2], Chongxin Luo[3], and Yao Cheng[4]

[1]State Key Laboratory of Estuarine and Coastal Research, East China Normal University, Shanghai, China, [2]Center for Marine Environmental Study, Ehime University, Matsuyama, Japan, [3]Key Laboratory of Marine Environment and Ecology, Ministry of Education, Ocean University of China, Qingdao, China, [4]School of Water Conservancy and Hydroelectric Power, Hebei University of Engineering, Handan, China

Key Points:
- The tidal effect on the water export rate in the eastern shelf seas of China (ESSC) is assessed from a timescale perspective
- Average water residence time in the ESSC is 2.12 years and reduces to 0.64 year if tides are excluded in the hydrodynamic model
- There is a high spatial variability of the tidal effect on the water export rate, which is associated with the water depth

Correspondence to:
L. Lin and D. Liu,
llin@sklec.ecnu.edu.cn;
dyliu@sklec.ecnu.edu.cn

Citation:
Lin, L., Liu, D., Guo, X., Luo, C., & Cheng, Y. (2020). Tidal effect on water export rate in the eastern shelf seas of China. *Journal of Geophysical Research: Oceans*, *125*, e2019JC015863. https://doi.org/10.1029/2019JC015863

Received 9 NOV 2019
Accepted 28 MAR 2020
Accepted article online 04 APR 2020

Abstract Water export rate of shelf seas is a pivotal factor impacting the global carbon cycle. Tides have important impacts on shelf hydrodynamics but are excluded in many climate models. To assess the effect of tides on export rates of shelf water, this study used a regional hydrodynamic model and a water residence time (WRT) adjoint model and examined model runs with and without tides for the eastern shelf seas of China. The results show that the average WRTs in the Bohai, Yellow, and East China seas were 11.60, 4.95, and 0.39 years, respectively. When tides were excluded, the WRTs decreased by >70% in the Bohai and Yellow seas and by ~10% in the East China Sea, indicating a significant acceleration in the shelf water export due to the absence of tides. The tidal effect has spatial variability associated with the water depth. Sensitivity experiments suggest that the tidal effect on the mean WRT was stronger than the effect of other dynamical factors (winds, rivers, and boundary currents). In the model with tides, tides weakened the wind-driven coastal current by intensifying the bottom resistance and thus slowed water export in the inner and middle portions of the shelf, compared to the model without tides. Parameterization of the tidal bottom friction in the model without tides could significantly improve the WRT result. This study highlights the crucial role of tides on the long-term transport of shelf seas and the significance of parameterizing the effect of tidal friction in climate models.

Plain Language Summary The export of water with a high carbon content to the deep oceans from shelf seas is a pivotal process impacting the global carbon cycle. Tides play an important role in the hydrodynamics of shelf seas and thus influence the water export. Hence, a quantitative assessment of the tidal effect on the water export rate is essential, in order to understand the role of tides in the global carbon cycle. Using water residence time (WRT) as an indicator and numerical modeling, this study finds that the model without tides decreased the WRT of the eastern shelf seas of China (ESSC) to ~1/3 compared to the model with tides, indicating a significant effect of tides on the water export from shelf seas. Meanwhile, the tidal effect on the water export in the ESSC was much stronger in the inner and middle shelves compared with that in the outer shelf. The findings of this study highlight the crucial impact of tides on the water exchange between shelf seas and deep oceans, which implies that small timescale and space-scale processes should be simulated or effectively parameterized in climate models in order to accurately predict the ocean and climate change.

1. Introduction

Due to the high primary productivity, shelf seas (especially in temperate zones) usually act as net carbon sinks (Cai et al., 2006; Thomas, 2004). Shelf seas exporting water with a high carbon content to the deep oceans is a pivotal process that impacts the global carbon cycle (Bauer et al., 2013; Cai et al., 2006; Holt et al., 2009; Laruelle et al., 2018; Regnier et al., 2013; Thomas, 2004; Walsh, 1991). An accurate simulation of water export rates from shelf seas is therefore critical for the accurate representations and projections of the global carbon cycle and climate change. However, hydrodynamic processes in shelf seas cannot usually be well represented in climate models due to their small spatial scale compared to the global ocean (Graham et al., 2018; Holt et al., 2017). In particular, as one of the major motions in shelf seawater, tides are either excluded or parameterized in many climate models given their significantly shorter timescales in comparison to those of climate, in addition to numerical stability problems (Holt et al., 2017; Lee et al., 2006;

Luneva et al., 2015; Müller et al., 2010; Simmons et al., 2004; Voldoire et al., 2013). Therefore, it is significant and necessary to quantitatively evaluate the tidal effect on the water export rate of shelf seas.

Tides can modulate shelf currents through affecting water mixing and bottom friction (e.g., Moon et al., 2009; Palma et al., 2004; Wang et al., 2013; Wu et al., 2018). Tides can also influence the water transport by inducing residual currents, which is especially important for the nearshore water (e.g., Cai et al., 2014; Delhez, 1996; Feng et al., 2008; Lin et al., 2015; Wu et al., 2018). In these ways, tides could have a significant influence on the shelf hydrodynamics and thus on the water export rate. For instance, in the Ross Sea, tides enhanced the cross-shelf exchange and the Antarctic bottom water export (Wang et al., 2010; Whitworth & Orsi, 2006), which suggests that tides could accelerate the shelf water export. However, numerical experiments conducted for the Southwestern Atlantic Shelf suggested that tides could weaken the shelf currents (Palma et al., 2004), which suggests that tides could inhibit the shelf water export. The opposite effects suggest that the tidal effect on the shelf water export rate should be of high spatial heterogeneity.

Water transport at the shelf break or at key transects is often used to quantify the shelf water export rate (e.g., Graham et al., 2018; Wang et al., 2013; Zhou et al., 2015), which is essential for understanding local water exchanges. However, water transport cannot depict well the spatial variability of the water export rate over an entire shelf. For instance, the water export rate in an inner shelf is related not only to the cross-shelf transport at the shelf break but also to the hydrodynamics in the inner and middle shelves. Therefore, the spatial variability of the tidal effect on the water export rate on a shelf cannot be accurately assessed using only the cross-sectional transport. In this study, we used the water residence time (WRT) to represent the water export rate on the shelf. WRT is defined as the time a water parcel needs to leave the region of interest for the first time (Bolin & Rodhe, 1973; Delhez et al., 2004; Takeoka, 1984). WRT provides a timescale approach for summarizing the complex dynamics of a system and can reflect the spatial variability of the water export rate over shelf seas and quantify the retention timescale of coastal water that constrains the coast-ocean exchange (e.g., Liu et al., 2019).

The eastern shelf seas of China (ESSC), which include the Bohai Sea (BS), the Yellow Sea (YS), and the East China Sea (ECS), are one of the widest continental shelves in the world (Figure 1a). The ESSC cover an area of more than 122×10^4 km^2, with an average water depth of ~240 m (Su & Yuan, 2005). Strong tides occur in the ESSC, and semidiurnal tidal constituents (M_2 and S_2) are predominant (e.g., Guo & Yanagi, 1998). This study uses a regional hydrodynamic model and timescale diagnosis to examine the tidal effect on the WRT in the ESSC, with the overall aim of better understanding the tidal effect on the water export rate over the ESSC and its spatiotemporal variability. Hence, we anticipate that our findings will provide a reference material for climate and Earth system modeling.

This paper is organized as follows. The hydrodynamic and WRT diagnosis models and the numerical experiment schemes are introduced in section 2. Section 3 shows the results of the WRT of the ESSC and the tidal effect on the WRT. In section 4, the effect of the reentry process is evaluated, and the mechanism of the tidal effect on the WRT and its implications for climate modeling are discussed. At last, a brief conclusion is given in section 5.

2. Methods

2.1. Study Area

The ESSC connect rivers from eastern China (including the Changjiang River, the third longest river in the world) and the western Korea Peninsula with the western Pacific Ocean (Figure 1a). The ESSC represent a vital carbon storage area and export ~15.25–36.70 $\times 10^9$ kg of organic carbon per year to the Pacific (Jiao et al., 2018). The circulation system in the ESSC is basically composed of the Kuroshio along the shelf break, the Taiwan warm current, the Yellow Sea warm current (YSWC) (in winter), and coastal currents that are forced by the Asian monsoon winds (Figure 1b). The seasonal variability in water transport across the shelf break and its dynamic mechanism in the ESSC have been previously studied using ocean models or in situ observations (e.g., Ding et al., 2016; Guo et al., 2006; Zhou et al., 2015). Findings from these studies are very helpful for understanding the local water export rate along the shelf break, while this study aims to provide an understanding of the water export rate of the entire ESSC from a timescale perspective.

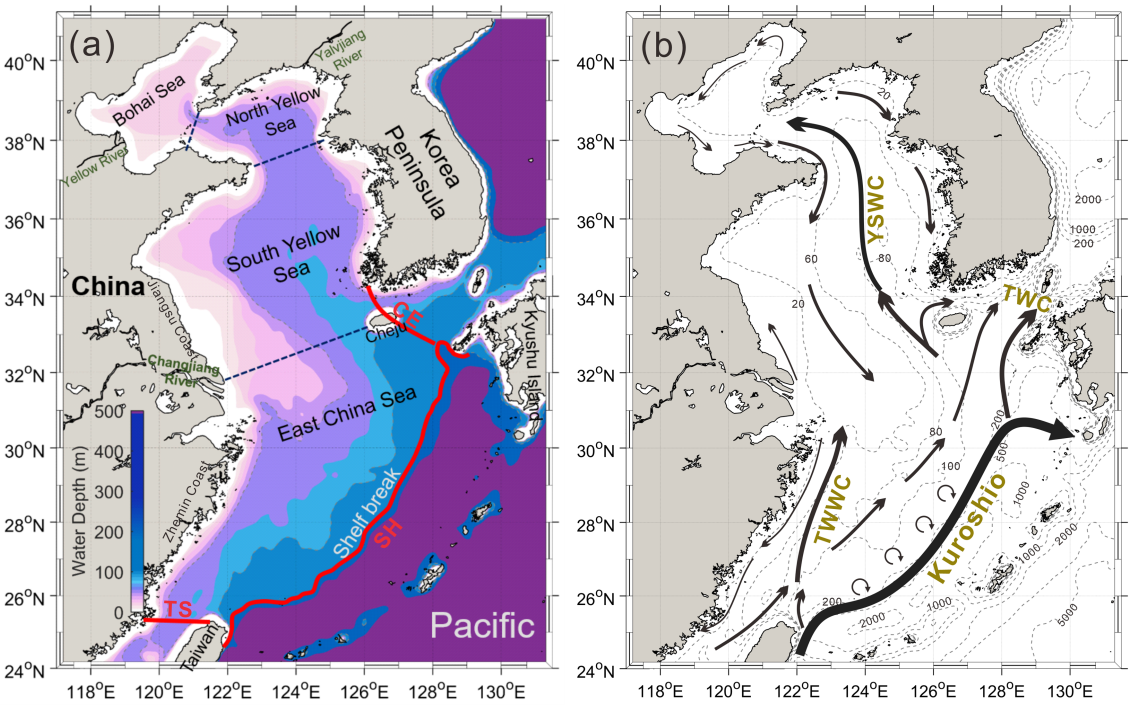

Figure 1. (a) Topography and the model domain of the eastern shelf seas of China (ESSC). The red lines denote the prescribed open boundary of the control region for the calculation of WRT. (b) Primary circulation pattern for the ESSC in winter. TWWC: Taiwan warm current; TWC: Tsushima warm current; YSWC: Yellow Sea warm current. The gray dotted lines are the isobaths (m).

2.2. Hydrodynamic Model

A hydrodynamic model of the ESSC was initially developed by Guo et al. (2003) based on the Princeton Ocean Model (Blumberg & Mellor, 1987; Mellor, 1998) and a triple-nesting method. Wang et al. (2008) added tidal forcing (including M_2, S_2, K_1, and O_1 tidal constituents) into the finest grid model and used a smaller model domain (117.5–131.5°E and 24.0–41.0°N) covering the ESSC (Figure 1a), which is also used in this study. The model domain is discretized by a grid space of 1/18 degree (~5–6 km) in the horizontal direction and 21 sigma levels in the vertical direction. The time steps for the external and internal modes in the model are 9 and 360 s, respectively.

To focus on the results of climatological state, the model is driven by climatological mean monthly forcings, including winds, heat flux, precipitation and evaporation rates, and river runoff (Guo et al., 2003; Wang et al., 2008). A more detailed description and validation of the hydrodynamic model are provided in Guo et al. (2003, 2006), Wang et al. (2008), and Zhu et al. (2018). This model has been applied by Liu et al. (2012) to study the water age of the Yellow River in the BS, by Zhu et al. (2018) to study the interannual variation in the YS cold water mass, by Zhao and Guo (2011) to study cross-shelf transport of nutrients in ECS, and by Zhang et al. (2019) to study the role of nutrients with different origins in the primary production in the ECS. These studies demonstrated that the model presented a good representation of the hydrodynamic characteristics of ESSC. Following a 3-year spin-up, the model outputted data of the sea level, three velocity components, and the horizontal and vertical diffusivity coefficients with a time interval of 0.5 hr over 1 year to drive the WRT diagnostic model (section 2.3).

2.3. Diagnosis of WRT

Since WRT is the time that a water parcel needs to leave the region of interest for the first time, it follows that a longer WRT means a slower water export. In this study, the 200-m isobath along the shelf break, which is usually regarded as the open boundary of the cross-shelf exchange in the ESSC (e.g., Ding et al., 2016; Guo et al., 2006; Zhou et al., 2015), was set as the boundary of the region of interest for WRT (red line labeled SH

Table 1
Boundary Conditions for the WRT Equation and Model

Boundary conditions	Expressions
Open boundary of ω	$\overline{\theta} = 0$
Closed boundary of ω	$\vec{\mathbf{n}}\cdot(\nabla\overline{\theta}) = 0$
Boundaries of the computational domain	$\overline{\theta} = 0$

Note. $\vec{\mathbf{n}}$ is the outgoing unit vector normal to the boundary.

in Figure 1a). To close the region of interest, we added two "gates" at the Taiwan Strait (TS) and to the east of Cheju Island (CE) (Figure 1a).

The adjoint method proposed by Delhez et al. (2004) was used to determine the spatiotemporal distribution of WRT in the ESSC. By solving the adjoint problem of the tracer transport, Delhez et al. (2004) derived the spatiotemporal variation in WRT using equation 1:

$$\left\{\frac{\partial\overline{\theta}}{\partial t} + \delta_\omega(\mathbf{x}) + \mathbf{v}\cdot\nabla\overline{\theta} + \nabla\cdot\left[\mathbf{K}\cdot\nabla\overline{\theta}\right] = 0\delta_\omega(\mathbf{x}) = \begin{cases} 1 & \forall\mathbf{x}\in\omega \\ 0 & \forall\mathbf{x}\notin\omega \end{cases}\right., \quad (1)$$

where $\overline{\theta}$ denotes WRT, $\mathbf{v}$ is the velocity field, $\mathbf{K}$ is the diffusivity tensor, and $\delta_\omega(\mathbf{x})$ is the characteristic function of the control region ω. To solve WRT, equation 1 should be integrated backward in time (Delhez et al., 2004). The initial field is set to 0 for $\overline{\theta}$ (Delhez, 2006). As listed in Table 1, a homogenous Dirichlet boundary condition, $\overline{\theta} = 0$, is prescribed at the open boundaries of the control region (Delhez et al., 2004). The impermeability boundary condition, $\vec{\mathbf{n}}\cdot(\nabla\overline{\theta}) = 0$, is used at the mouth of the estuaries, because in the hydrodynamic model, the river discharges are treated as downward water flux at sea surface over the river grids, that is, by the corresponding increase in precipitation at these grids (Wang et al., 2008). In the hydrodynamic model, this type of boundary condition for river runoff may underestimate the momentum at the estuarine regions. However, wind-driven currents are the dominance on the shelf, and the underestimation of the momentum will not significantly affect the water transport in the ESSC. In addition, the experiment results show that the impact of the river boundary condition on the WRT in ESSC is unlikely to be very significant (see section 3.2). Therefore, this issue is believed to be a minor one for this study.

The WRT diagnostic model established by Lin and Liu (2019a) and Liu et al. (2016) based on equation 1 is used in this study. The WRT model is solved using the finite-difference method with the same domain, grids, and layers as the ESSC hydrodynamic model. The second-order centered difference is applied to solve the diffusion terms. A second-order total variation diminishing scheme with alternating Superbee and MUSCL flux limiters (TVDal, Lin & Liu, 2019b) is used to solve the advection terms. Using the climatological velocity and diffusion coefficients from the hydrodynamic model, we ran the WRT diagnostic model for 30 years to complete the spin-up when a stable interannual variation of WRT in the ESSC was obtained and the effect of the initial condition on the WRT disappeared (Delhez & Deleersnijder, 2006; Du & Shen, 2016). The WRT value of the 30th year was used for the analysis.

2.4. Sensitivity Experiments

To examine the tidal effect on the WRT in the ESSC, we conducted a numerical sensitivity experiment, in which the tides were excluded from the hydrodynamic model. Following a 3-year spin-up of the hydrodynamic model without tides, the WRT in the ESSC was diagnosed with the same procedures described in section 2.3 (hereafter termed "NoTide case"). In addition, to compare the importance of tides with other dynamic factors, that is, local winds, river runoff, and boundary currents (BCs), we carried out another three sensitivity experiments. Two of these were similar to NoTide case but where winds and river runoff were excluded instead, respectively (hereafter termed "NoWind case" and "NoRiver case," respectively). The third sensitivity experiment reduced the flow velocity at the southern and eastern open boundaries to half of their original values (hereafter termed "HalfBC case"). WRTs of different cases were compared with the control run (with the complete set of forcings) to quantify the effect of each dynamic factor on the water export rate in the ESSC.

3. Results

3.1. WRT in the ESSC

The WRTs in the ESSC that were obtained from the control run are shown in Figure 2a. The annual mean WRT in the ESSC was 2.12 years. The annual mean WRTs of the BS, YS, and ECS were 11.60, 4.95 (7.01 and 4.56 for the north and south YS, respectively), and 0.39 years, respectively. The model results agreed with the estimated WRT based on the isotopic observations from previous studies (e.g., Chen, 1997; Kim et al., 2005; Nozaki et al., 1991; Tsunogai et al., 1997). For instance, using Ra-226 and Ra-228 isotopes and their

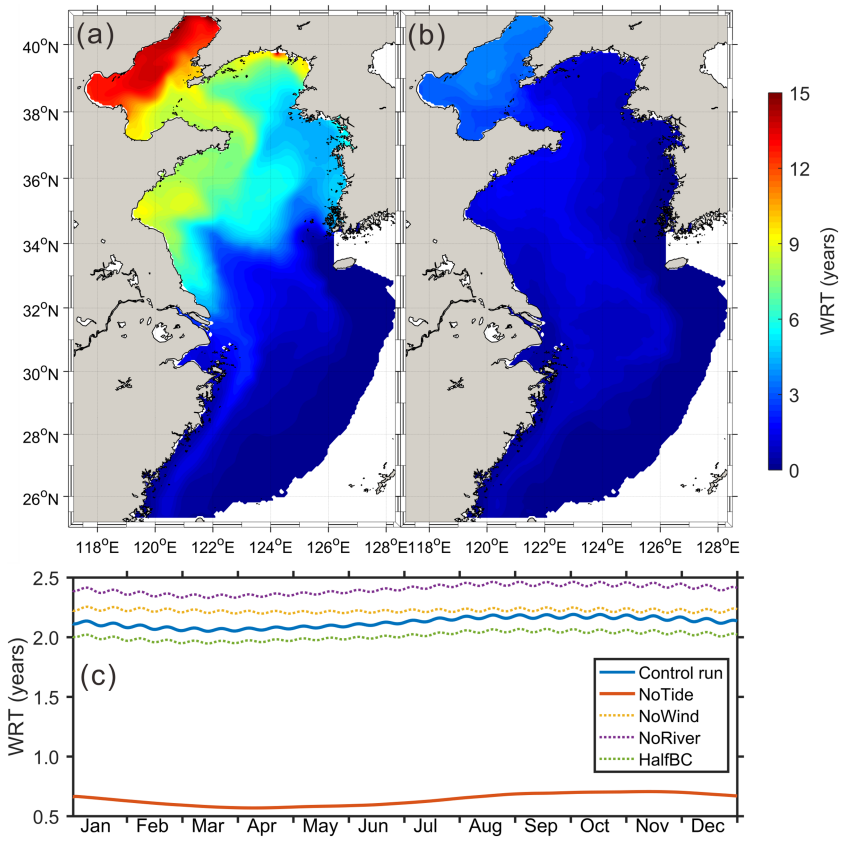

Figure 2. The annual mean of vertically averaged WRT in the ESSC for (a) the control run and (b) the NoTide case, (c) The daily mean WRTs over the ESSC for the five cases.

mass-balance models, Kim et al. (2005) and Nozaki et al. (1991) derived an average WRT of 4.9 and 5–6 years for water in the south YS, respectively, both of which are very close to our WRT of 4.56 years. Based on the mean inventory of excess alkalinity, Tsunogai et al. (1997) and Chen (1997) estimated a WRT of 0.8 ± 0.3 and 1.3 ± 0.4 years for the ESC continental shelf water, respectively, which are much shorter than the WRT in the south YS. In addition, the WRT in the BS is ~4 years longer than that in the north YS, thus indicating that the water in the BS requires around 4 years to leave the BS, which is consistent with the mean water age of the Yellow River water at the BS strait (~3.4 years) derived from another modeling study (Liu et al., 2012). Therefore, the WRT diagnostic model applied in this study is considered to be reliable.

Spatially, the WRTs increased from the outer shelf to the inner shelf (Figure 2a). The WRT of the 100-m isobath was <1 year, increasing to <3 years in the ECS, 3–10 years in the YS, and up to ~15 years in the BS. The WRTs at the estuaries can approximately indicate the average time required for the river water to leave the ESSC. The modeled annual mean WRTs at the estuaries of the three major rivers along the coast of the ESSC (i.e., the Changjiang, Yellow, and Yalvjiang rivers) were 2.70, 11.01, and 9.25 years, respectively.

Compared to the annual mean, the seasonal variation in the spatial mean WRT was relatively small (Figure 2c). Average WRTs in the ESSC were shortest during March (~2.06 years) and longest during September (~2.17 years). A relatively significant seasonal variation in the WRT occurred at the Jiangsu Coast and the Korea West Coast (Figure 3), which could be related to the seasonal variation in the coastal currents dominated by the monsoon winds. In addition, WRTs showed a fortnightly variation with an averaged magnitude of ~0.03 year, which corresponded to the spring-neap tidal variation (Figure 2c). The WRTs in the ESSC were vertically homogenous during the winter and autumn due to vigorous vertical mixing. During the spring and summer, WRTs showed a slight vertical change due to stratification (Figure 4).

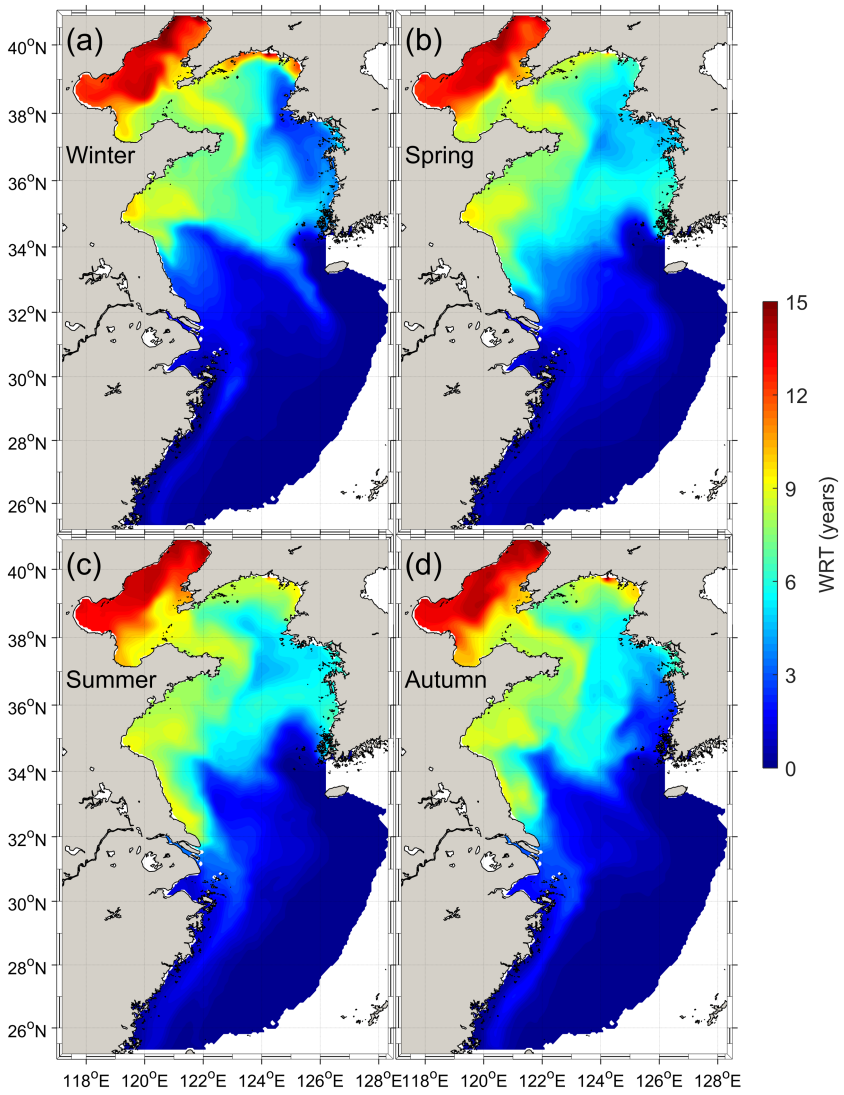

Figure 3. Vertically averaged WRT in the ESSC in summer, autumn, winter, and spring.

3.2. Tidal Effect on the WRT in the ESSC

Compared to the control run, the WRT reduced greatly when tides were excluded from the hydrodynamic model (Figure 2b). The annual mean WRTs in the ESSC for the NoTide case were shorter than 4 years throughout the ESSC (Figure 2b). The average WRT in the ESSC was <0.71 year over a year, with an annual mean of 0.64 year, which was only ~1/3 of that obtained in the control run (2.12 years). This reduction in the WRT indicates that the water export rate in the ESSC increased by more than three times on average when tides were excluded. For the NoTide case, the annual mean WRTs in the BS, YS, and ECS were 3.27, 1.02 (1.24 and 0.98 for the north and south YS, respectively), and 0.35 years, respectively. These represent decreases of 72%, 79%, and 10%, respectively, compared to the control run. For the estuaries of the Changjiang, Yellow, and Yalvjiang rivers, the WRTs for the NoTide case were 0.54, 3.05, and 1.16 years, respectively. These represent reductions of 80%, 72%, and 87%, respectively, compared to the control run. As expected, the fortnightly variation in the WRTs was not found in the NoTide case, while the weak seasonal variation remained (Figure 2c).

The relative difference between the annual mean WRTs of the control run and the NoTide case was calculated to understand the spatial variability of the tidal effect on the shelf water export rate. As shown in Figure 5a, a significant decrease in the WRTs occurred on the inner and middle shelves (water depth

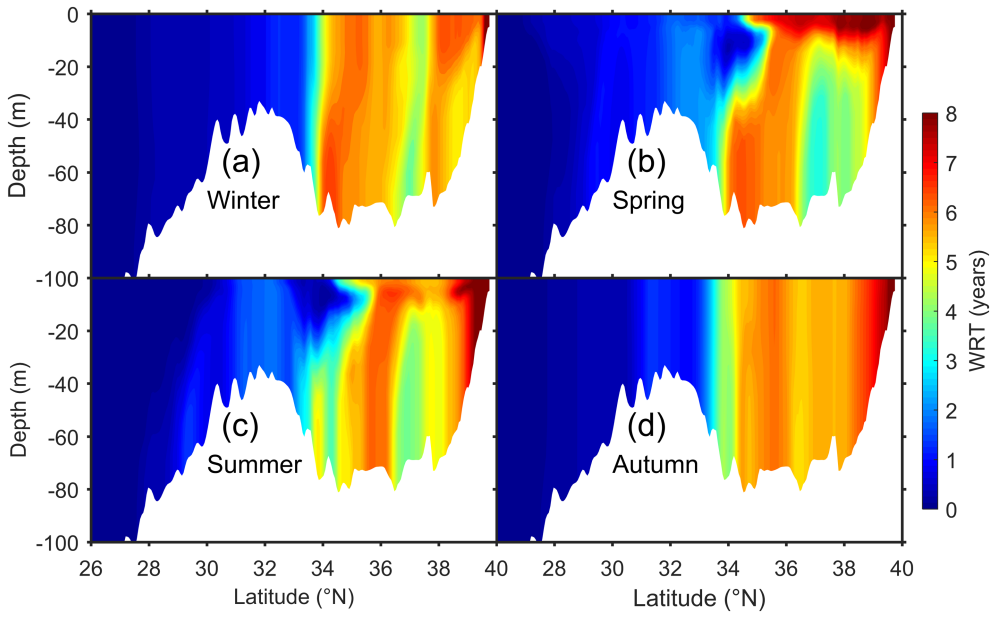

Figure 4. WRT along the transect of 124°E in summer, autumn, winter, and spring.

generally <80 m). The WRT change was relatively small on the outer shelf except that the WRT increased at the central ECS (see the dashed circle in Figure 5a). As shown in Figure 5b, tides increased WRT at water depth roughly <80 m, and the tidal effect on the WRT became stronger as the water depth got shallower. The tidal effect became opposite in the relatively deep water (the water depth >80 m), but it was weaker than the tidal effect on the shallow water (also see Figure 5a). The good correlation between the relative difference and the water depth indicates that the tidal effect on the water export rate in ESSC is highly related to the water depth.

The sensitivity experiments also show that the average WRTs in the ESSC for the NoWind, HalfBC, and NoRiver cases were 2.22, 2.00, and 2.40 years, respectively (Figures 2c and 6). These values were close to the WRTs obtained from the control run. When compared to the control run, the relative changes in these three cases were <15%, which is far less than that in the NoTide case (~70%). These results indicate that tides have a dominant impact on the WRT in the ESSC.

Although the spatially averaged WRTs in the ESSC obtained in the NoWind case were close to that obtained in the control run, their spatial distributions of WRTs were significantly different (Figure 6). Without winds, the WRTs increased in the BS and north YS but decreased in the south YS, thus indicating that local winds affected the spatial pattern of WRTs in the ESSC. To focus on the tidal effect on WRT, this study will not discuss the impact of winds on the WRT.

4. Discussion

4.1. The Impact of the Reentry Process on the Results

The concept and diagnosis method of the WRT was used to quantify the water export rate in ESSC according to the Constituent-oriented Age and Residence time Theory (Deleersnijder et al., 2001; Delhez & Deleersnijder, 2002; Delhez et al., 2004). The WRT results show that there is a significant difference in the water export rate between the ocean models with and without tides. WRT is defined as the time that a water parcel needs to leave the region of interest for the first time. The use of WRT means that the boundary prescribed in this study represented a strict one to separate the shelf sea and the deep ocean and the effect of the reentry process is ignored (Delhez et al., 2004). This can be interpreted as that once a water parcel crosses the

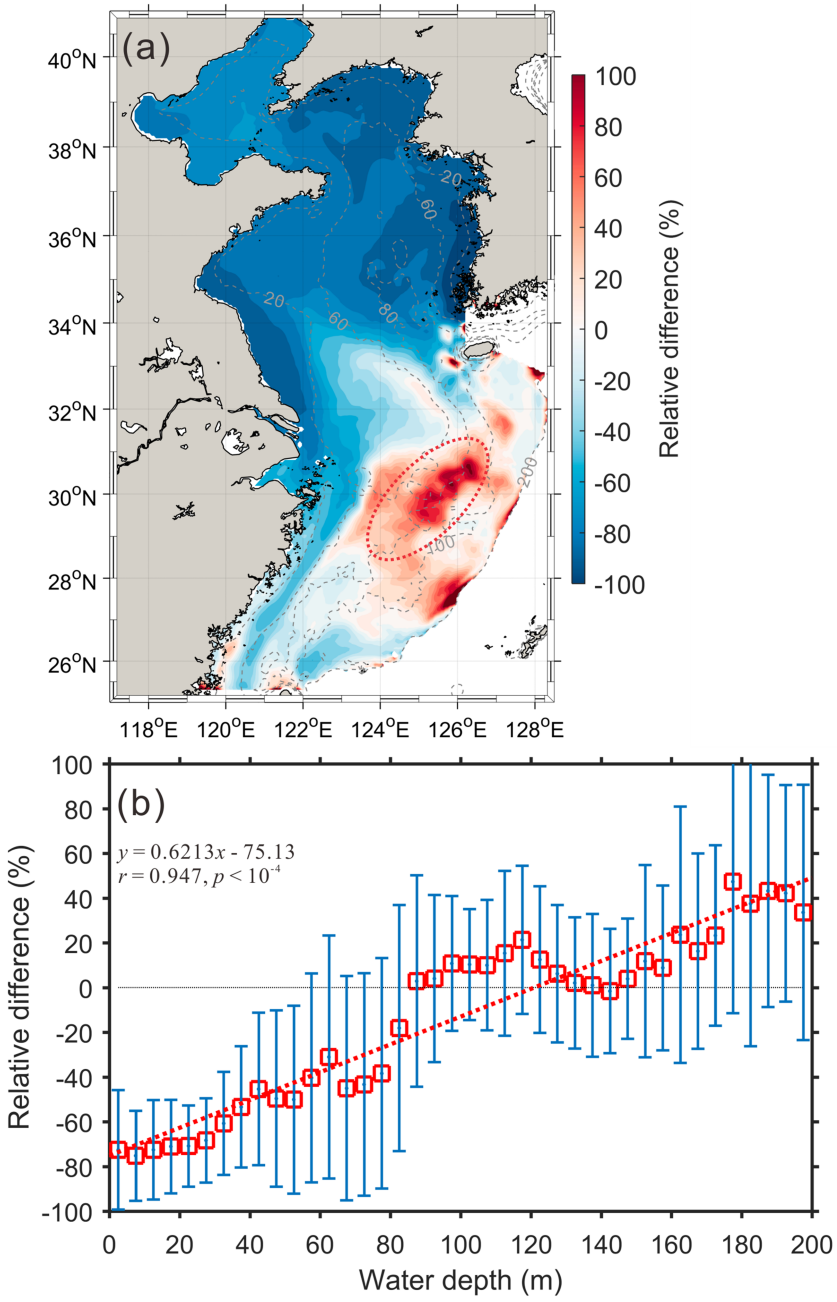

Figure 5. (a) The relative difference in the annual mean WRT between the control run and NoTide case. Negative (positive) values denote the WRT decreased (increased) percent of the NoTide case compared to the control run. The gray dotted lines are the isobaths. (b) The relative difference in the annual mean WRT varying with the water depth with an interval of 5 m. The red squares denote the mean values, and the blue error bars denote their standard deviations. The red dotted line is the linear regression for the mean values, and the regression equation is labeled at the top left corner.

boundary, its property will change from shelf water to oceanic water due to mixing and highly altered biogeochemical processes.

In some cases, the water parcel could reenter the control region due to the effect of return flows at the open boundary of the shelf sea. To assess the effect of the reentry process on the results, we calculated the water exposure time (WET) and then the return coefficient r introduced by de Brauwere et al. (2011), which defined as

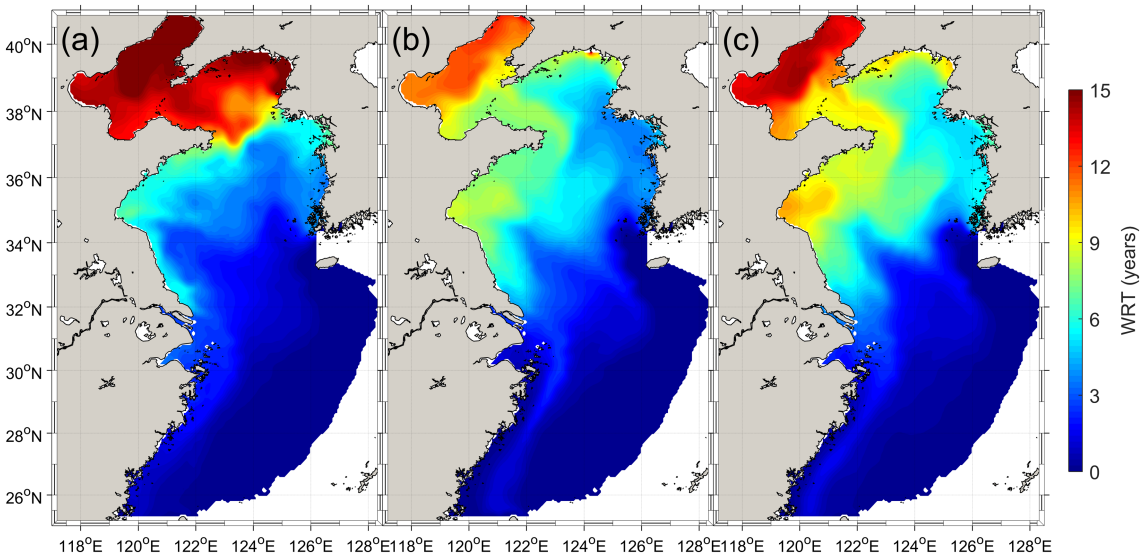

Figure 6. The annual mean of vertically averaged WRTs in the ESSC for three sensitivity experiments: (a) NoWind case; (b) HalfBC case (i.e., half flow velocity at the southern and eastern open boundaries); and (c) NoRiver case.

$$r = (\mathrm{WET} - \mathrm{WRT})/\mathrm{WET}. \tag{2}$$

WET measures the total time spent in the ESSC as the water parcel leaves and reenters the region of interest (de Brye et al., 2012; Delhez, 2013). The equation of the WET is the same as that of the WRT except that no boundary conditions need to be prescribed on the open boundaries of the control region (de Brye et al., 2012; Delhez, 2013). The return coefficient r is comprised between 0 and 1. The larger the value of r, the stronger the effect of the reentry process on the water transport timescale.

Figure 7a shows that the WET in ESSC had a very similar spatial pattern with the WRT. The annual mean WET in the ESSC was 2.38 years and slightly higher than WRT (2.12 years), indicating that the reentry process could prolong the time that seawater spent on the shelf for 0.26 year on average. The return coefficient was basically less than 0.2 on the inner and middle shelves, with a relatively large value ($r > 0.5$) at the outer shelf. The result suggests that the effect of the reentry process is more significant on the outer shelf, especially near the open boundary (Figure 7b). For the NoTide case, the WET with an annual mean of 0.66 year was very close to the WRT (Figure 7c). The mean return coefficient for the NoTide case was 0.03, which was much less than that of the control run (0.11), indicating that the tidal current could be the dominant dynamics driving the water mass to return to the shelf. Moreover, the WET of the control run was 3.6 times as long as that of the NoTide case, indicating that the tidal effect on the water export rate will be more significant if considering the reentry process.

4.2. The Role of Tidal Mixing and Intensified Bottom Friction in the WRT

In order to examine the effect of tidally induced mixing and tidally intensified bottom friction on the WRT in the ESSC, two extra numerical experiments were conducted. In one experiment, tides were excluded, but the vertical eddy viscosity and diffusivity coefficients from the control run were used (hereafter termed "TM case"). In the other experiment, linear bottom friction with parameterization of the tidal effect on the bottom stress used by Lee et al. (2000) and Moon et al. (2009) was applied (hereafter termed "BF case"). In the control run, the bottom friction stress, $\vec{\tau}_b$, in momentum equations of seawater motion that was used in the hydrodynamic model was derived from the quadratic law as defined by equation 3:

$$\vec{\tau}_b = \rho C_d \left|\vec{V}\right| \vec{V}, \tag{3}$$

where ρ is the water density, C_d is the friction coefficient, and $\vec{V}$ is the instantaneous velocity. In BF case, instead of the quadratic bottom friction, a linear-type bottom friction stress was applied to parameterize the enhanced bottom friction due to tidal stress, as defined by equation 4:

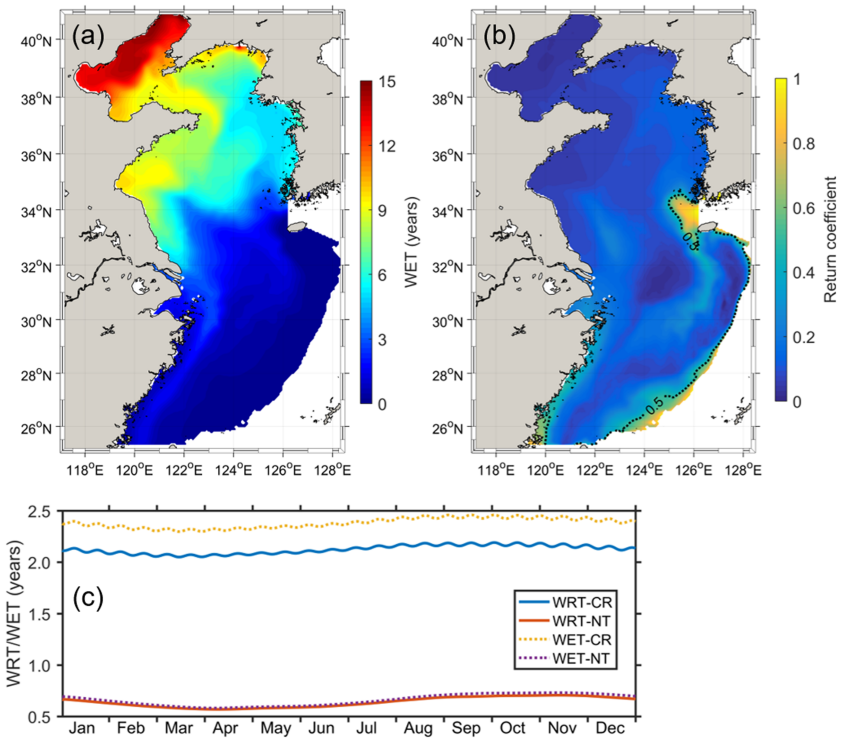

Figure 7. The annual mean of (a) vertically averaged water exposure time (WET) and (b) the return coefficient in the ESSC for the control run. (c) The daily mean WRTs and WETs over the ESSC for the control run (-CR) and the NoTide case (-NT).

$$\vec{\tau}_b = \rho C_d k \vec{V}, \tag{4}$$

where k is the coefficient of the linear bottom friction. According to Lee et al. (2000) and Moon et al. (2009), the coefficient k can be calculated using equation 5:

$$k = 1.23\sqrt{U_T^2 + V_T^2}, \tag{5}$$

where U_T and V_T are the amplitude components of the depth-averaged M_2 tidal currents, which are derived from the velocity field of the control run.

The extra experiment results showed that WRTs in the TM case were very close to that obtained in the NoTide case (Figures 8a, 8c, and 8d), thus indicating that the impact of tidal mixing on the shelf water export rate was limited. The annual mean WRT in the BF case increased significantly compared to the WRT obtained for the NoTide case, and it was ~0.47 year lower than that obtained in the control run (Figures 8b and 8c). However, there is still a remarkable difference in the spatial distribution of WRT between the BF case and the control run (Figure 8e), which may be related to the absence of the residual tidal current and the interaction between tidal currents and shelf currents in the BF case. These results suggest that the tidally intensified bottom friction has a more important effect on the water export rate than the tidal mixing in the ESSC. The parameterization of the tidal effect on the bottom friction in hydrodynamic models can reduce the bias of the mean water export rate for the model without tides, but it can still induce considerable biases in some areas on the shelf.

4.3. Impact of Tides on the Shelf Circulation in the ESSC

The sensitivity experiments showed that tides significantly affect the WRTs over the ESSC. The water export in shelf seas is determined by advection and turbulence mixing. The results of the TM case suggest that the effect of the altered mixing on WRT is limited. Therefore, the effect of the tides on the shelf current should be the main cause of the significant differences in the WRTs between the control run and the NoTide case.

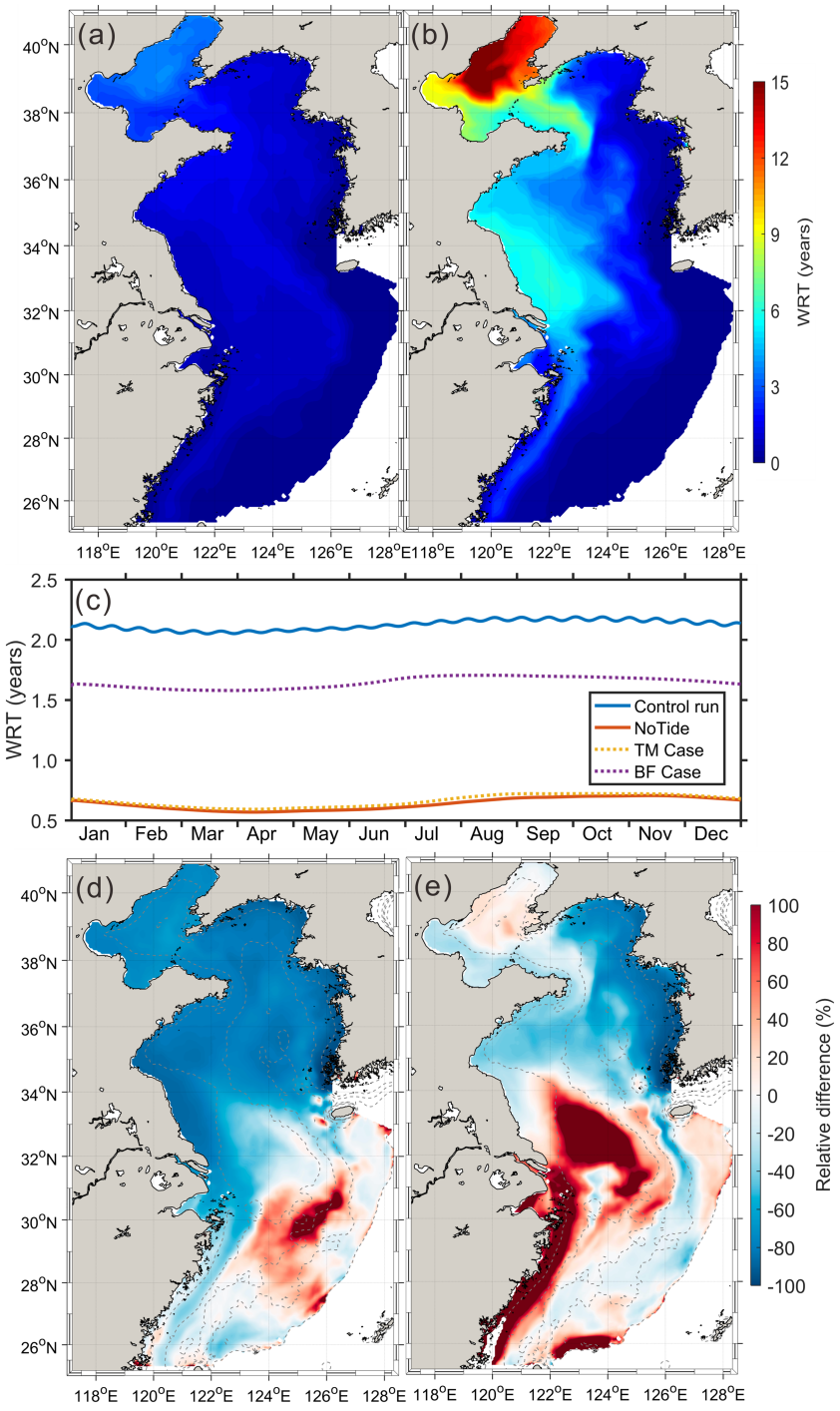

Figure 8. The annual mean of vertically averaged WRTs in the ESSC for the (a) TM case and (b) BF case. (c) The daily data of the averaged WRT in the ESSC in the TM and BF cases along with those in the control run and the NoTide case. (d) The relative difference in the annual mean WRT between the control run and TM case. (e) The relative difference in the annual mean WRT between the control run and BF case.

Here, we analyze the impact of the tides on cross-shelf transport and shelf currents in the ESSC in order to understand the tidal effect on the water export rate in the ESSC.

As shown in Figure 9, the water transport across a zonal transect in the YS during the control run and the NoTide case were remarkably different. When compared to the control run, the outflow across the 36°N

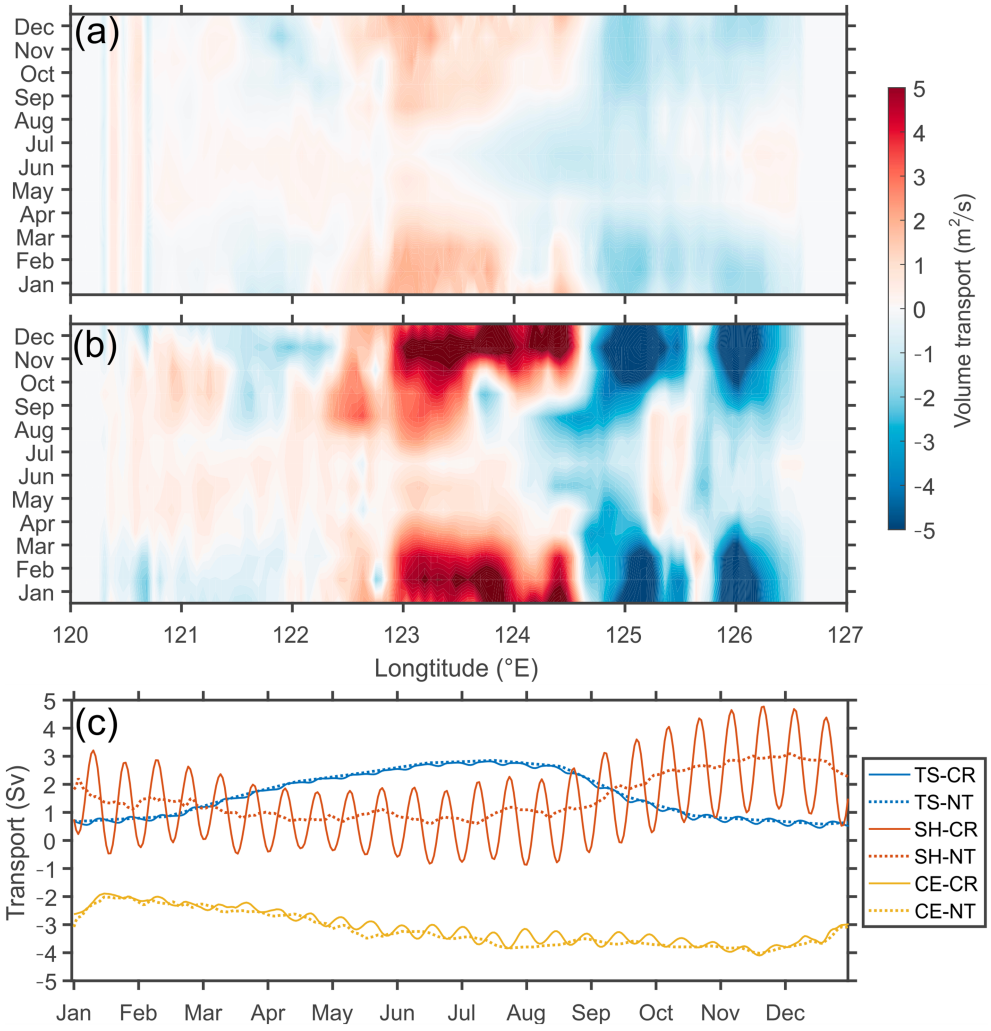

Figure 9. Monthly transport (per unit width) across the zonal transect of 36°N in the Yellow Sea (YS) for (a) the control run and (b) the NoTide case. (c) Daily mean transport over a year across three transects (TS, SH, and CE in Figure 1a) of the open boundary of the ESSC for the control run (-CR) and NoTide case (-NT). Positive and negative values for the transport denote inflow and outflow, respectively.

transect in the NoTide case increased by ~2.5 times over the year (Figures 9a and 9b), which explains the significant reduction in the WRT in the YS and BS. The increase in the outflow was more pronounced during the winter half-year (from October to March), which accounted for ~73% of the volume transport for the entire year in the NoTide case. However, the impact of tides on water transport at the shelf boundary of the ESSC was limited. Figure 9c shows that the transports across the three transects of the open boundary for the NoTide case were very close to those obtained during the control run. The annual mean outflow/inflow for the NoTide case was ~3.2 Sv (1 Sv = 10^6 m^3/s), which was only ~5% higher than that for the control run (~3.05 Sv). This explains the relatively small change in the WRTs in the ECS in the NoTide case.

The remarkable difference in the transport across the transect in the YS between the control run and NoTide case relates to the effect of tidal modulation on the circulation system of the YS. As shown in Figure 10, the circulation intensities in the YS and BS decreased markedly in the presence of tides, especially during winter. For the control run, the magnitude of the mean velocities in the YS and BS during the winter was basically <0.05 m/s, which agrees with the results of field observations and previous modeling studies (e.g., Lin &

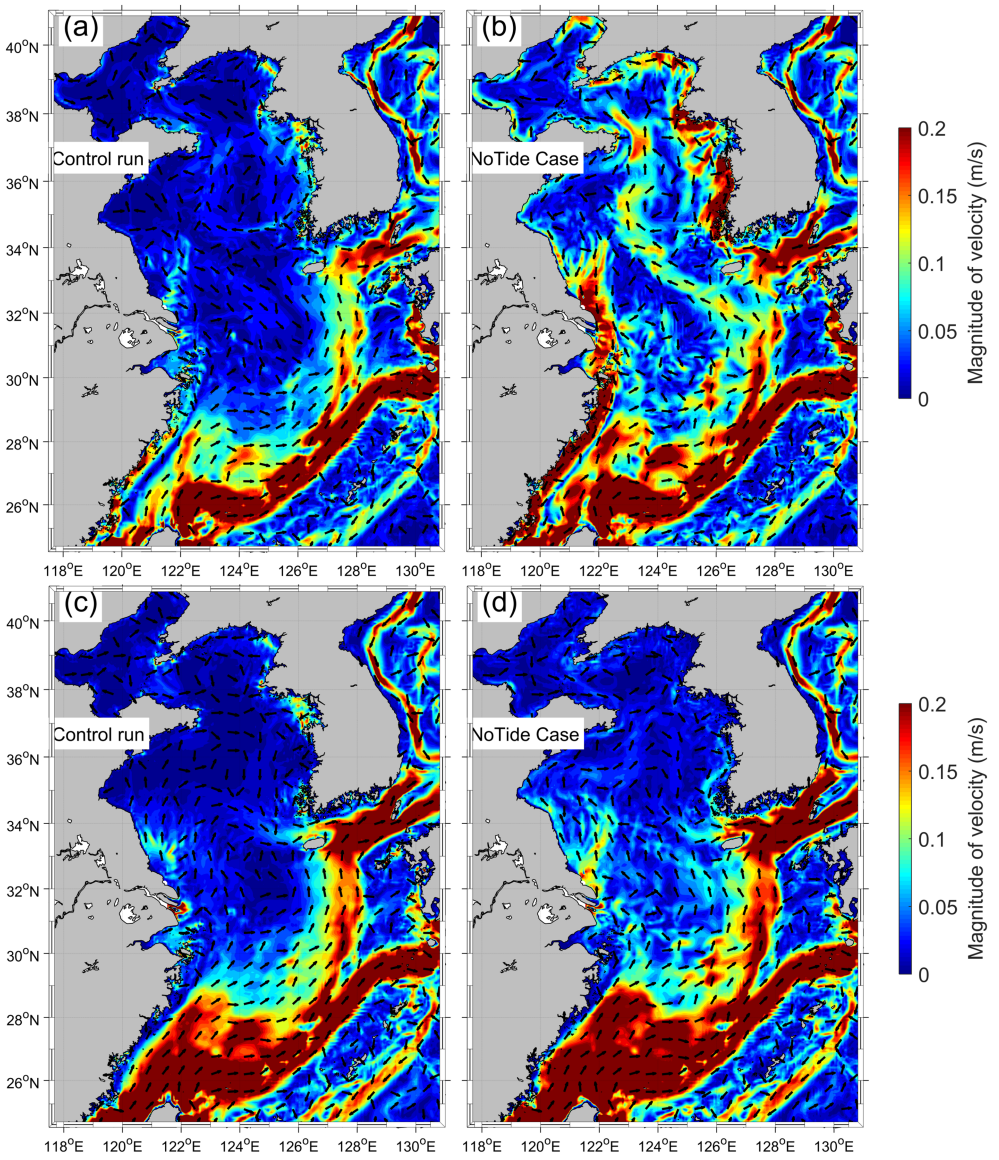

Figure 10. Monthly mean velocity (vertically averaged, m/s) in February (a and b) and August (c and d) in the ESSC for the control run and the NoTide case, respectively.

Yang, 2011; Lin et al., 2011; Ma et al., 2006). By contrast, the coastal currents in the YS, BS, and the YSWC for the NoTide case reached 0.1–0.2 m/s, which was much stronger than of those in the control run (Figures 10a and 10b). The stronger coastal currents and the YSWC were also reproduced by models without tides in Huang et al. (2005) and Moon et al. (2009). For the ECS, the Zhemin coastal current was also intensified in the NoTide case, whereas the tidal effect on the Kuroshio and other currents in the ECS was not as significant as the effect on the currents in the YS and BS.

The significant enhancement of the coastal currents and the YSWC in the NoTide case facilitated the water exchange of the BS and YS and accelerated the water export from the YS and BS into the ECS, where water exchange was faster. Therefore, the WRTs in the ESSC were greatly reduced in the NoTide case, although the water transport at the open boundary of the ESSC did not increase significantly. The results indicate that the water export rate in the inner and middle shelves was strongly related to the local hydrodynamics and that water transport across the shelf boundary is more representative of the local water exchange rather than the

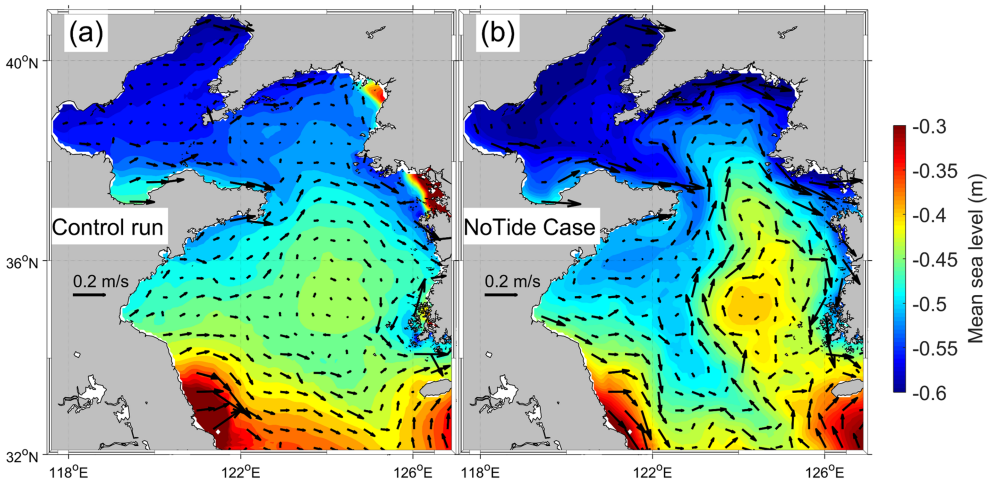

Figure 11. Monthly mean sea level and geostrophic flows (arrows) in February in the Bohai Sea (BS) and the Yellow Sea (YS) for (a) the control run and (b) the NoTide case. Geostrophic flows were diagnosed using the barotropic geostrophic balance (e.g., Cushman-Roisin & Beckers, 2011).

water exchange rate over the entire shelf sea. When tides were excluded in the model, the simulated YSWC was significantly enhanced, which could bring more ECS water into the YS. Therefore, in the NoTide case, some water in the ECS could be staying longer in the shelf rather than be directly transported through the open boundaries. This could explain the WRT increase at the central ECS in the NoTide case (Figure 5a).

The difference in the magnitude of coastal currents in ESSC between the control run and the NoTide case is mainly related to the tidal effect on the bottom friction, which is supported by the results of the BF experiment in section 4.2. When tides are included in the model, the tidal mean bottom resistance could increase by approximately one order of magnitude in coastal waters due to the nonlinear tidal effect on bottom friction stress (e.g., Parker, 1991; Wu & Wu, 2018). The intensified bottom resistance caused by tides could counteract wind stress, which dramatically weakens the wind-driven coastal currents (e.g., Moon et al., 2009; Palma et al., 2004; Wu & Wu, 2018). The reduction of coastal currents in the BS and YS induced a relatively small sea-level gradient for the YS that led to a relatively weak barotropic geostrophic current in the central YS (Figure 11). Thus, the YSWC was weaker in the control run than in the NoTide case. The reduction of the shelf currents by tides induced a slower water exchange in the shelf in the control run and thus increased the WRTs in the YS and BS. On the other hand, tides have been reported to decelerate and even reverse the wind-induced coastal currents via a tidal residual current (Lie & Cho, 2016; Moon et al., 2009; Wu & Wu, 2018), which could be important for the YS current during the summer (Moon et al., 2009). For the ECS, due to the relatively deep water depth (average ~80 m), the influence of the change in the bottom friction on the shelf current was weaker than that of in the YS and BS, and thus, the tidal effect on the water export rate was relatively small.

4.4. Implications for Climate Modeling

The results of this study showed the spatial variability of the tidal effect on the water export rate on the shelf. The variability of tidal effects could be associated with the water depth of the shelf seas. For relatively shallow shelves such as the inner and middle shelves in ESSC and Southwestern Atlantic Shelf (water depth mostly <100 m), bottom stress usually plays a major role in the momentum balance (Palma et al., 2004). Tides enhance bottom friction resistance and therefore reduce the velocity of shelf currents and slow the shelf water export. However, for relatively deep shelves, the tidal effect on the shelf water export even can be opposite. For instance, in the studies conducted in the Ross Sea (~500- to 700-m average water depth), Whitworth and Orsi (2006) and Wang et al. (2013) found that tides facilitated the shelf water outflow to some extent. The geostrophic balance and the baroclinic current are commonly dominant in the deep water. The influence of tides on the water density structure

becomes vital for the tidal modulation of shelf currents. Spatial variations in tidal mixing and tidal advection could intensify the horizontal density gradients and thus increase the baroclinic current, which could be favorable for water transport, for example, in the Ross Sea (Wang et al., 2010, 2013). Although the impacts of tides on shelf water export are complicated, considering the tidal effect is essential for correctly simulating the process of shelf water export in climate models. Meanwhile, the results of the extra experiments in section 4.2 show that the parameterization of tidal bottom friction could improve the water export rate of the entire shelf sea for the models without tides. However, due to the difference in the spatial distribution of WRTs between the models with the parameterized tides and the explicitly described tides, the test and comparison of different parameterizations of the tidal effect on the bottom friction should be pursued in the following studies. Moreover, the effect of the oscillating tidal currents on the water export rate still needs to be quantified for understanding the potential of the improvement on the model by tidal parameterization.

Besides the tides, other high-frequency phenomena, for example, diurnal forcing, or small-scale processes could influence the hydrodynamics in shelf seas (e.g., Graham et al., 2018; Yu et al., 2017) and thus on the water export from shelf seas to deep oceans. In this study, monthly mean forcings were used in the hydrodynamic model to characterize the shelf circulation in the ESSC and drive the WRT model. An extra experiment with six hourly forcings (winds and heat fluxes) shows that the average change in the WRT was ~17% compared to the monthly mean forcings (the results of this numerical experiment were not presented in order to focus on the tidal effect), which suggest that the forcing frequency could also have some influences on the water export rate in ESSC, although much weaker than that of the tides. Therefore, more attention should be paid to the effect of high-frequency processes and forcings in climate models, in spite of their small-time and small-space scales.

Shallow shelves are especially important for the global carbon cycle. For instance, Dunne et al. (2007) estimated that depths shallower than 50 m could account for 48% of the global flux of organic carbon to the seafloor. The significant tidal effect on the water export rate from shelf seas implies that tides could play an important role in shelf carbon export and climate models that do not consider the tidal effect could overestimate the carbon export rate from shallow shelves to the deep oceans. Nevertheless, in the future, it will be necessary to couple the hydrodynamic model with a biogeochemical model so as to enable a more thorough analysis of the impacts of tides on shelf carbon export to the deep oceans.

5. Conclusions

Using the WRT as an indicator and a regional hydrodynamic model, we quantitively evaluated the tidal effect on the water export rate in the ESSC. The model results show that the average WRT in the ESSC was 2.12 years, which decreased to 0.63 year when tides were removed from the hydrodynamic model. This suggests a significant effect of tides on the modeled water export rate from the shelf. The tidal effect on the WRTs in the inner and middle shelves (roughly water depth <80 m) was >70%, which was much stronger than that in the outer shelf (~10%), thereby indicating a high spatial variability of the tidal effect on the water export rate across the shelf. Compared to the case without tides, it is the significantly weakened shelf circulation in the inner and middle shelves in the case with tides that slows the water export rate in the shelf, while the change in the water transport across the shelf boundary in the cases with and without tides is very limited. This can explain the stronger effect of tides on the inner and middle shelves than the outer shelf. The effect of tidal mixing on the WRT in ESSC was very small, while the effect of tides on the bottom friction was a dominant factor for the tidal effect on the WRT. When tides are included in the model, they intensified bottom resistance and thus decreased coastal currents. The reduced coastal currents induce a smaller gradient of the water level across the shelf and thus a weaker YSWC in winter in the control case than in the case without tides. The reduced coastal currents and YSWC in the YS and BS therefore induced a much slower water exchange and water export rate for the inner and middle shelves compared to the case without tides. The results of this study imply that there could be a considerable simulation error for the water exchange between shelf seas and deep oceans in the climate and Earth system models that do not consider the tidal effect, which could introduce biases in the projections of the global carbon cycle.

Appendix A: List of Abbreviations

WRT	Water residence time
WET	Water exposure time
ESSC	The eastern shelf seas of China
BS	The Bohai Sea
YS	The Yellow Sea
ECS	The East China Sea
TS	The Taiwan Strait
SH	Shelf break
CE	The east of Cheju Island
YSWC	Yellow Sea Warm Current
TVDal	Total variation diminishing scheme with an alternating flux limiter
CART	Constituent-oriented Age and Residence time Theory

Acknowledgments
This study was supported by the China Postdoctoral Science Foundation (Project 2017M621409), the National Natural Science Foundation of China (Grants 41706011 and 41876127), and the Ministry of Science and Technology, China (2016YFE0133700 and 2016YFA0600904). The authors would like to thank the two anonymous reviewers for their very constructive comments that helped us improve the manuscript. Original data used for the figures are available at https://doi.org/10.6084/m9.figshare.11788917.

References

Bauer, J. E., Cai, W., Raymond, P. A., Bianchi, T. S., Hopkinson, C. S., & Regnier, P. A. G. (2013). The changing carbon cycle of the coastal ocean. *Nature*, *504*(7478), 61–70. https://doi.org/10.1038/nature12857

Blumberg, A. F., & Mellor, G. L. (1987). A description of a three-dimensional coastal ocean circulation model. *Coastal and Estuarine Sciences*, *4*, 1–16.

Bolin, B., & Rodhe, H. (1973). A note on the concepts of age distribution and transit time in natural reservoirs. *Tellus*, *25*(1), 58–62.

Cai, W., Dai, M., & Wang, Y. (2006). Air-sea exchange of carbon dioxide in ocean margins: A province-based synthesis. *Geophysical Research Letters*, *33*, L12603.

Cai, Z., Liu, Z., Guo, X., Gao, H., & Wang, Q. (2014). Influences of intratidal variations in density field on the subtidal currents: Implication from a synchronized observation by multiships and a diagnostic calculation. *Journal of Geophysical Research: Oceans*, *119*(3), 2017–2033.

Chen, C. T. (1997). The Kuroshio intermediate water is the major source of nutrients on the East China Sea continental shelf. *Oceanographic Literature Review*, *5*(44), 531.

Cushman-Roisin, B., & Beckers, J. M. (2011). Introduction to geophysical fluid dynamics: Physical and numerical aspects (vol. 101). *Academic Press*.

de Brauwere, A., De Brye, B., Blaise, S., & Deleersnijder, E. (2011). Residence time, exposure time and connectivity in the Scheldt estuary. *Journal of Marine Systems*, *84*(3–4), 85–95.

de Brye, B., de Brauwere, A., Gourgue, O., Delhez, E. J., & Deleersnijder, E. (2012). Water renewal timescales in the Scheldt estuary. *Journal of Marine Systems*, *94*, 74–86.

Deleersnijder, É., Campin, J. M., & Delhez, É. J. M. (2001). The concept of age in marine modelling I. Theory and preliminary model results. *Journal Marine Systems*, *28*(2), 29–267.

Delhez, É. J. (2013). On the concept of exposure time. *Continental Shelf Research*, *71*, 27–36.

Delhez, É. J. M. (1996). On the residual advection of passive constituents. *Journal of Marine Systems*, *8*(3–4), 147–169.

Delhez, É. J. M. (2006). Transient residence and exposure times. *Ocean Science*, *2*(1), 1–9.

Delhez, É. J. M., & Deleersnijder, É. (2002). The concept of age in marine modelling: II. Concentration distribution function in the English Channel and the North Sea. *Journal of Marine Systems*, *31*(4), 279–297.

Delhez, É. J. M., & Deleersnijder, É. (2006). The boundary layer of the residence time field. *Ocean Dynamics*, *56*(2), 139–150.

Delhez, É. J. M., Heemink, A. W., & Deleersnijder, É. (2004). Residence time in a semi-enclosed domain from the solution of an adjoint problem. *Estuarine, Coastal and Shelf Science*, *61*(4), 691–702.

Ding, R., Huang, D., Xuan, J., Mayer, B., Zhou, F., & Pohlmann, T. (2016). Cross-shelf water exchange in the East China Sea as estimated by satellite altimetry and in situ hydrographic measurement. *Journal of Geophysical Research: Oceans*, *121*(9), 7192–7211.

Du, J., & Shen, J. (2016). Water residence time in Chesapeake Bay for 1980–2012. *Journal of Marine Systems*, *164*, 101–111.

Dunne, J. P., Sarmiento, J. L., & Gnanadesikan, A. (2007). A synthesis of global particle export from the surface ocean and cycling through the ocean interior and on the seafloor. *Global Biogeochemical Cycles*, *21*(4).

Feng, S., Ju, L., & Jiang, W. (2008). A Lagrangian mean theory on coastal sea circulation with inter-tidal transports I. Fundamentals. *Acta Oceanologica Sinica*, *27*(6), 1–16.

Graham, J. A., Rosser, J. P., O'Dea, E., Hewitt, H. T. (2018). Resolving shelf break exchange around the European northwest shelf. *Geophysical Research Letters*, *45*(22), 12, 312–386, 395.

Guo, X., Hukuda, H., Miyazawa, Y., & Yamagata, T. (2003). A triply nested ocean model for simulating the Kuroshio—Roles of horizontal resolution on JEBAR. *Journal of Physical Oceanography*, *33*(1), 146–169.

Guo, X., Miyazawa, Y., & Yamagata, T. (2006). The Kuroshio onshore intrusion along the shelf break of the East China Sea: The origin of the Tsushima warm current. *Journal of Physical Oceanography*, *36*(12), 2205–2231.

Guo, X., & Yanagi, T. (1998). Three-dimensional structure of tidal current in the East China Sea and the Yellow Sea. *Journal of Oceanography*, *54*(6), 651–668.

Holt, J., Hyder, P., Ashworth, M., Harle, J., Hewitt, H. T., Liu, H., et al. (2017). Prospects for improving the representation of coastal and shelf seas in global ocean models. *Geoscientific Model Development*, *10*(1), 499–523.

Holt, J., Wakelin, S., & Huthnance, J. (2009). Down-welling circulation of the northwest European continental shelf: A driving mechanism for the continental shelf carbon pump. *Geophysical Research Letters*, *36*, L14602.

Huang, D., Fan, X., Xu, D., Tong, Y., & Su, J. (2005). Westward shift of the Yellow Sea warm salty tongue. *Geophysical Research Letters*, *32*, L24613.

Jiao, N., Liang, Y., Zhang, Y., Liu, J., Zhang, Y., Zhang, R., et al. (2018). Carbon pools and fluxes in the China seas and adjacent oceans. *Science China Earth Sciences*, *61*(11), 1535–1563.

Kim, G., Ryu, J., Yang, H., & Yun, S. (2005). Submarine groundwater discharge (SGD) into the Yellow Sea revealed by ^{228}Ra and ^{226}Ra isotopes: Implications for global silicate fluxes. *Earth and Planetary Science Letters*, *237*(1–2), 156–166.

Laruelle, G. G., Cai, W., Hu, X., Gruber, N., Mackenzie, F. T., & Regnier, P. (2018). Continental shelves as a variable but increasing global sink for atmospheric carbon dioxide. *Nature Communications*, *9*(1).

Lee, H., Rosati, A., & Spelman, M. J. (2006). Barotropic tidal mixing effects in a coupled climate model: Oceanic conditions in the northern Atlantic. *Ocean Modelling*, *11*(3–4), 464–477.

Lee, H. J., Jung, K. T., Foreman, M. G. G., & Chung, J. Y. (2000). A three-dimensional mixed finite-difference Galerkin function model for the oceanic circulation in the Yellow Sea and the East China Sea. *Continental Shelf Research*, *20*(8), 863–895.

Lie, H. J., & Cho, C. H. (2016). Seasonal circulation patterns of the Yellow and East China seas derived from satellite-tracked drifter trajectories and hydrographic observations. *Progress in Oceanography*, *146*, 121–141.

Lin, L., & Liu, Z. (2019a). Partial residence times: Determining residence time compositions in different subregions. *Ocean Dynamics*, *69*(9), 1023–1036. https://doi.org/10.1007/s10236-019-01298-8

Lin, L., & Liu, Z. (2019b). TVDal: Total variation diminishing scheme with alternating limiters to balance numerical compression and diffusion. *Ocean Modelling*, *134*, 42–50.

Lin, L., Liu, Z., Xie, L., Gao, H., Cai, Z., Chen, Z., & Zhao, J. (2015). Dynamics governing the response of tidal current along the mouth of Jiaozhou Bay to land reclamation. *Journal of Geophysical Research: Oceans*, *120*, 2958–2972.

Lin, X., & Yang, J. (2011). An asymmetric upwind flow, Yellow Sea warm current: 2. Arrested topographic waves in response to the northwesterly wind. *Journal of Geophysical Research*, *116*, 5.

Lin, X., Yang, J., Guo, J., Zhang, Z., Yin, Y., Song, X., & Zhang, X. (2011). An asymmetric upwind flow, Yellow Sea warm current: 1. New observations in the western Yellow Sea. *Journal of Geophysical Research*, *116*, 28–33.

Liu, X., Dunne, J. P., Stock, C. A., Harrison, M. J., Adcroft, A., & Resplandy, L. (2019). Simulating water residence time in the coastal ocean: A global perspective. *Geophysical Research Letters*, *46*, 13,910–13,919.

Liu, Z., Lin, L., Xie, L., & Gao, H. (2016). Partially implicit finite difference scheme for calculating dynamic pressure in a terrain-following coordinate non-hydrostatic ocean model. *Ocean Modelling*, *106*, 44–57.

Liu, Z., Wang, H., Guo, X., Wang, Q., & Gao, H. (2012). The age of Yellow River water in the Bohai Sea. *Journal of Geophysical Research*, *117*, 317–323.

Luneva, M. V., Aksenov, Y., Harle, J. D., & Holt, J. T. (2015). The effects of tides on the water mass mixing and sea ice in the Arctic Ocean. *Journal of Geophysical Research: Oceans*, *120*, 6669–6699.

Ma, J., Qiao, F., Xia, C., & Chang, S. K. (2006). Effects of the Yellow Sea warm current on the winter temperature distribution in a numerical model. *Journal of Geophysical Research*, *111*, 201–219.

Mellor, G. L. (1998). *Users guide for a three dimensional, primitive equation, numerical ocean model*. Princeton, NJ: Program in Atmospheric and Oceanic Sciences, Princeton University.

Moon, J. H., Hirose, N., & Yoon, J. H. (2009). Comparison of wind and tidal contributions to seasonal circulation of the Yellow Sea. *Journal of Geophysical Research*, *114*.

Müller, M., Haak, H., Jungclaus, J. H., Sündermann, J., & Thomas, M. (2010). The effect of ocean tides on a climate model simulation. *Ocean Modelling*, *35*(4), 304–313.

Nozaki, Y., Tsubota, H., Kasemsupaya, V., Yashima, M., & Naoko, I. (1991). Residence times of surface water and particle-reactive ^{210}Pb and ^{210}Po in the East China and Yellow seas. *Geochimica et Cosmochimica Acta*, *55*(5), 1265–1272.

Palma, E. D., Matano, R. P., & Piola, A. R. (2004). A numerical study of the Southwestern Atlantic Shelf circulation: Barotropic response to tidal and wind forcing. *Journal of Geophysical Research*, *109*.

Parker, B. B. (1991). The relative importance of various nonlinear mechanisms in a wide range of tidal interactions. In B. B. Parker (Ed.), *Tidal hydrodynamics*, (pp. 237–268). New York, NY: John Wiley & Sons.

Regnier, P., Friedlingstein, P., Ciais, P., Mackenzie, F. T., Gruber, N., Janssens, I. A., et al. (2013). Anthropogenic perturbation of the carbon fluxes from land to ocean. *Nature Geoscience*, *6*(8), 597.

Simmons, H. L., Jayne, S. R., Laurent, L. C. S., & Weaver, A. J. (2004). Tidally driven mixing in a numerical model of the ocean general circulation. *Ocean Modelling*, *6*(3–4), 245–263.

Su, J. L., & Yuan, Y. L. (2005). *Hydrology in China shelf seas (in Chinese)*. Beijing: Ocean Press.

Takeoka, H. (1984). Fundamental concepts of exchange and transport time scales in a coastal sea. *Continental Shelf Research*, *3*(3), 311–326.

Thomas, H. (2004). Enhanced open ocean storage of CO_2 from shelf sea pumping. *Science*, *304*(5673), 1005–1008. https://doi.org/10.1126/science.1095491

Tsunogai, S., Watanabe, S., Nakamura, J., Ono, T., & Sato, T. (1997). A preliminary study of carbon system in the East China Sea. *Journal of Oceanography*, *53*(1), 9–17.

Voldoire, A., Sanchez-Gomez, E., y Mélia, D. S., Decharme, B., Cassou, C., Sénési, S., et al. (2013). The CNRM-CM5.1 global climate model: Description and basic evaluation. *Climate Dynamics*, *40*(9–10), 2091–2121.

Walsh, J. J. (1991). Importance of continental margins in the marine biogeochemical cycling of carbon and nitrogen. *Nature*, *350*(6313), 53.

Wang, Q., Danilov, S., Hellmer, H., Sidorenko, D., Schroeter, J., & Jung, T. (2013). Enhanced cross-shelf exchange by tides in the western Ross Sea. *Geophysical Research Letters*, *40*(21), 5735–5739.

Wang, Q., Danilov, S., Hellmer, H. H., & Schröter, J. (2010). Overflow dynamics and bottom water formation in the western Ross Sea: Influence of tides. *Journal of Geophysical Research*, *115*.

Wang, Q., Guo, X., & Takeoka, H. (2008). Seasonal variations of the Yellow River plume in the Bohai Sea: A model study. *Journal of Geophysical Research*, *113*.

Whitworth, T., & Orsi, A. H. (2006). Antarctic bottom water production and export by tides in the Ross Sea. *Geophysical Research Letters*, *33*.

Wu, H., Gu, J., & Zhu, P. (2018). Winter counter-wind transport in the inner southwestern Yellow Sea. *Journal of Geophysical Research: Oceans*, *123*(1), 411–436.

Wu, T., & Wu, H. (2018). Tidal mixing sustains a bottom-trapped river plume and buoyant coastal current on an energetic continental shelf. *Journal of Geophysical Research: Oceans*, *123*(11), 8026–8051.

Yu, Y., Gao, H., Shi, J., Guo, X., & Liu, G. (2017). Diurnal forcing induces variations in seasonal temperature and its rectification mechanism in the eastern shelf seas of China. *Journal of Geophysical Research: Oceans. 122*.

Zhang, J., Guo, X., & Zhao, L. (2019). Tracing external sources of nutrients in the East China Sea and evaluating their contributions to primary production. *Progress in Oceanography*, *176*.

Zhao, L., & Guo, X. (2011). Influence of cross-shelf water transport on nutrients and phytoplankton in the East China Sea: A model study. *Ocean Science*, *7*, 27.

Zhou, F., Xue, H., Huang, D., Xuan, J., Ni, X., Xiu, P., & Hao, Q. (2015). Cross-shelf exchange in the shelf of the East China Sea. *Journal of Geophysical Research: Oceans*, *120*(3), 1545–1572.

Zhu, J., Shi, J., Guo, X., Gao, H., & Yao, X. (2018). Air-sea heat flux control on the Yellow Sea cold water mass intensity and implications for its prediction. *Continental Shelf Research*, *152*, 14–26.